arXiv:2301.12822v1 [cs.LG] 30 Jan 2023

Evaluating COVID-19 vaccine allocation policies using Bayesian m-top exploration

Alexandra Cimpean[1], Timothy Verstraeten[1], Lander Willem[3], Niel Hens[2,3], Ann Nowé[1], and Pieter Libin[1,2,4]

[1]Artificial Intelligence Lab, Department of Computer Science, Vrije Universiteit Brussel, Brussels, Belgium
[2]Data Science Institute, Interuniversity Institute of Biostatistics and statistical Bioinformatics, UHasselt, Hasselt, Belgium
[3]Centre for Health Economics Research and Modelling Infectious Diseases, Vaccine & Infectious Disease Institute, University of Antwerp, Antwerp, Belgium
[4]Rega Institute for Medical Research, Clinical and Epidemiological Virology, Department of Microbiology and Immunology, University of Leuven, Leuven, Belgium

Abstract

Individual-based epidemiological models support the study of fine-grained preventive measures, such as tailored vaccine allocation policies, *in silico*. As individual-based models are computationally intensive, it is pivotal to identify optimal strategies within a reasonable computational budget. Moreover, due to the high societal impact associated with the implementation of preventive strategies, uncertainty regarding decisions should be communicated to policy makers, which is naturally embedded in a Bayesian approach.

We present a novel technique for evaluating vaccine allocation strategies using a multi-armed bandit framework in combination with a Bayesian anytime m-top exploration algorithm. m-top exploration allows the algorithm to learn m policies for which it expects the highest utility, enabling experts to inspect this small set of alternative strategies, along with their quantified uncertainty. The anytime component provides policy advisors with flexibility regarding the computation time and the desired confidence, which is important as it is difficult to make this trade-off beforehand.

We consider the Belgian COVID-19 epidemic using the individual-based model STRIDE, where we learn a set of vaccination policies that minimize the number of infections and hospitalisations. Through experiments we show that our method can efficiently identify the m-top policies, which is validated in a scenario where the ground truth is available. Finally, we explore how vaccination policies can best be organised under different contact reduction schemes. Through these experiments, we show that the top policies follow a clear trend regarding the prioritised age groups and assigned vaccine type, which provides insights for future vaccination campaigns.

1 Introduction

Epidemiological models (e.g., compartment models and individual-based models) are essential to study the effects of preventive measures *in silico* [4, 20]. While individual-based models are typically associated with a greater model complexity and computational cost than compartment models, they allow for a more realistic evaluation of preventive strategies [12]. To capitalize on these advantages and to make it feasible to employ individual-based models, it is essential to use available computational resources as efficiently as possible.

In the literature, a set of possible preventive strategies is typically evaluated by simulating each of the strategies an equal number of times [17, 16, 10]. However, this approach is computationally inefficient to identify the optimal preventive strategies, as a large proportion of computational resources will be used to evaluate sub-optimal strategies. Furthermore, a consensus on the required number of model evaluations per strategy is currently lacking [55] and it was shown that this number depends on the *hardness* of the evaluation problem [35].

In this work, we present a novel technique to evaluate preventive strategies using a multi-armed bandit framework in combination with anytime m-top exploration algorithms. By formulating the decision problem as an m-top exploration bandit problem, a learning agent can select the m policies for which it expects the highest utility, enabling experts to inspect this small set of alternatives. The anytime component provides the policy advisors with flexibility regarding the time at which a decision is made. This is especially important when computationally intensive models are used, for which sample efficiency is essential. For such models it is difficult to make a trade-off between the available budget and desired confidence. We focus on a Bayesian learning approach, in order to quantify the uncertainty of the decision making.

As running an individual-based model is computationally intensive (i.e., minutes to hours, depending on the complexity of the model), minimizing the number of required model evaluations reduces the total time required to evaluate a given set of preventive strategies. This renders the use of individual-based models attainable in studies that would otherwise not be computationally feasible. Additionally, reducing the number of model evaluations will free up computational resources in studies that already use individual-based models, capacitating researchers to explore a larger set of model scenarios. This is important, as considering a wider range of scenarios increases the confidence about the overall utility of preventive strategies [56].

Using this novel framework, we investigate a vaccine allocation problem. We consider the Belgian COVID-19 epidemic [1], where we investigate how a weekly supply of vaccines is best allocated to the different age groups that make up the population, in a fine-grained individual-based model [54].

2 Related Work

Bayesian best-arm identification algorithms such as Top-two Thompson sampling have been used before to evaluate preventive strategies in the context of pandemic influenza [35]. When dealing with a fixed-budget problem, Top-two Thompson sampling is an appropriate algorithm as it increases exploration to minimize simple regret [42].

A broad overview on the state of the art with respect to (Bayesian) best-arm identification algorithms is provided by Kaufmann et al. and Hoffman et al. [27, 23]. Other settings attempt to identify the best arm with a predefined confidence: i.e., racing strategies [13], strategies that exploit the confidence bound of the arms' means [28] and more recently fixed confidence best-arm identification algorithms [19].

Epidemic control has been explored in a reinforcement learning setting [32], where deep reinforcement learning was used to learn mitigation strategies in the context of pandemic influenza. Reymond et al. explored COVID-19 mitigation policies from a multi-objective reinforcement learning perspective, where complex mitigation policies with possibly conflicting objectives are balanced to learn the best tradeoffs [41]. The concept to learn dynamic policies by formulating the decision problem as a Markov decision process (MDP) was first introduced by Yaesoubi and Cohen [57]. To investigate dynamic tuberculosis case-finding policies in HIV/tuberculosis co-epidemics, a policy iteration algorithm was used to solve the MDP [58]. This technique was later extended to include cost-effectiveness in the analysis and applied to mitigation policies (i.e., school closures and vaccines) in the context of pandemic influenza in a simplified epidemiological model [59].

Contextual multi-armed bandits have been used to learn effective vaccination strategies using a compartment model to simulate the COVID-19 epidemic [3]. However, this approach does not consider a computationally expensive model which requires efficient sampling. Moreover, this approach focuses on minimizing cumulative regret, whereas this work is based on *pure exploration* to find the top strategies. Grushka-Cohen et al. [21] presented a multi-armed bandit framework for efficiently dividing testing resources.

3 Methods

3.1 Epidemic bandits

We formulate the evaluation of preventive strategies as a multi-armed bandit problem [35] with the aim of identifying the m-top arms using anytime decision making algorithms [33]. The presented method is generic, capable of dealing with different epidemic model types, that consider distinct pathogens, contact networks and preventive strategies. This method will be evaluated in the context of COVID-19 in the next section.

First, we formally define the multi-armed bandit.

Definition 1 (Multi-armed bandit) A *multi-armed bandit* involves K arms that can be pulled [2], where each arm a_k returns a reward r_k when it is pulled, i.e., r_k represents a sample from a_k's *reward distribution*. For each arm a_k we have the expected reward $\mu_k = \mathbb{E}[r_k]$.

A common use of the multi-armed bandit is to pull a sequence of arms such that the best arm is identified. However, in this work, our aim is to solve the m-top exploration problem ($m < K$), where the objective is to identify the m best arms, with respect to the expected reward μ_k of the arms [5]. Formally, we have $\mu_1 \geq \ldots \geq \mu_m \geq \mu_{m+1} \geq \ldots \geq \mu_K$, and the objective is to identify the set $\{\mu_1, \ldots, \mu_m\}$. This is a *pure exploration* problem where the focus is on gaining knowledge about which m arms are ranked the highest.

Next, we provide a formal definition of the epidemic model we consider [35].

Definition 2 (Stochastic epidemiological model) A *stochastic epidemiological model* $\mathcal{E}$ is defined in terms of a model configuration $c \in \mathcal{C}$ and can be used to evaluate a preventive strategy p. The result of a model evaluation is referred to as the *model outcome*. Evaluating the model $\mathcal{E}$ thus results in a sample of the model's *outcome distribution*:

$$\text{outcome} \sim \mathcal{E}(c, p) \tag{1}$$

The model outcome can be any statistic relevant to the decision maker, e.g., prevalence, proportion of symptomatic individuals, proportion of hospitalised individuals, mortality, societal cost.

Note that a model configuration $c \in \mathcal{C}$ describes the complete model environment, i.e., both aspects inherent to the model and options that the modeller can provide (e.g., population statistics, vaccine properties).

Our objective is to find the set of top-m preventive strategies (i.e., the strategies that minimize the expected outcome) from a set of alternative strategies

$$\{p_1, ..., p_K\}, \tag{2}$$

for a particular configuration

$$c_0 \in \mathcal{C}, \tag{3}$$

where c_0 corresponds to the context of the studied epidemic. To this end, we consider a multi-armed bandit with

$$|\{p_1, ..., p_K\}| \tag{4}$$

arms. Pulling arm p_k corresponds to evaluating p_k by running a simulation in the epidemiological model $\mathcal{E}(c_0, p_k)$. The bandit thus has preventive strategies as arms with reward distributions corresponding to the outcome distribution of an epidemiological model $\mathcal{E}(c_0, p_k)$. While the parameters of the outcome distribution (i.e., the parameters of the epidemiological model) are known, it is intractable to determine the top strategies analytically. Hence, we must learn about the outcome distribution via interaction with the epidemiological model.

3.2 Top-m exploration

Our objective is to identify the top-m preventive strategies for a particular configuration of an epidemiological model. We consider two anytime top-m algorithms: AnyTime Lower and Upper Confidence Bound (AT-LUCB) and Boundary Focused Thompson Sampling (BFTS).

AnyTime Lower and Upper Confidence Bound algorithm

The AT-LUCB algorithm invokes the fixed-confidence LUCB algorithm [25, 26]. At each time step t, AT-LUCB (Algorithm 1) returns the empirical m-top arms $J^{(t)}$. Given K number of arms, $\hat{\mu}_a^t$ is the empirical mean for arm a at time step t. The amount of times arm a was pulled at time t is denoted by n_a^t. Given the LUCB stage index s, the confidence parameter at stage s is determined by a decaying failure parameter $\delta_s = \delta_1 \alpha^{s-1}$. The stage to which time t belongs is defined as $S^{(t)}$.

Algorithm 1: AT-LUCB

Input: $\delta_1 \leq [1/200, K]$, $\alpha \in [1/50, 1)$, $\epsilon \geq 0$

$S^{(0)} \leftarrow 1$
$\delta_s \leftarrow \delta_1 \alpha^{s-1}, \quad \forall s \geq 1$
for $t = 1, \ldots, +\infty$ **do**
  if $\text{Term}^t(\delta_{S^{(t-1)}}, \epsilon)$ **then**
    $S^{(t)} \leftarrow \max\{s' \geq S^{(t-1)} + 1 : \neg\text{Term}^t(\delta_{s'}, \epsilon)\}$
    $J^{(t)} \leftarrow \{\text{the empirical top-}m \text{ arms}\}$
  else
    $S^{(t)} \leftarrow S^{(t-1)}$
    $J^{(t)} \leftarrow J^{(t-1)}$ (or empirical top-m arms if $S^{(t)} = 1$)
  end
  Pull $h_*^t(\delta_{S^{(t)}})$ and $l_*^t(\delta_{S^{(t)}})$ as in Equation 7
  Recommend $J^{(t)}$
end

The exploration strategy of AT-LUCB relies on the upper confidence bound U_a^t and lower confidence bound L_a^t:

$$\begin{aligned} U_a^t(\delta_s) &= \hat{\mu}_a^t + \beta(n_a^t, t, \delta_s) \\ L_a^t(\delta_s) &= \hat{\mu}_a^t - \beta(n_a^t, t, \delta_s), \end{aligned} \tag{5}$$

with,

$$\beta(n_a^t, t, \delta_s) = \sqrt{\frac{1}{2n_a^t} \ln\left(\frac{5}{4}\frac{K \cdot t^4}{\delta_s}\right)}. \tag{6}$$

Each time step t, the algorithm pulls arms

$$\begin{aligned} h_*^t(\delta_{S^{(t)}}) &= \arg \min_{a \in \text{High}^t} L_a^t(\delta) \\ l_*^t(\delta_{S^{(t)}}) &= \arg \max_{a \in \text{High}^t} U_a^t(\delta), \end{aligned} \tag{7}$$

with High^t the top-m arms at time $t-1$. When the terminating condition $\text{Term}^t(\delta, \epsilon) = \{U^t_{l^t_*(\delta)}(\delta) - L^t_{h^t_*(\delta)}(\delta) < \epsilon\}$ is met, the algorithm moves to the next stage.

Boundary Focused Thompson Sampling

While confidence bound algorithms such as AT-LUCB permit specifying tight theoretical bounds, algorithms based on Thompson sampling typically perform better in practice [11]. Thompson sampling uses samples of the bandit's posteriors to decide which arm to pull next.

By using a Bayesian m-top identification algorithm, prior knowledge about the outcome distributions can be taken into account when defining an appropriate prior and posterior on the arms' reward distributions. This prior knowledge can increase the sample efficiency while the resulting posteriors provide valuable information about the decision uncertainty to guide policy makers.

For a multi-armed bandit, our prior belief over the arms' means is given by a prior distribution $\pi(.)$. Given an observed history $\mathcal{H}^{t-1}$ of rewards r from pulling arms a until timestep $t-1$, where

$$\mathcal{H}^{t-1} = \left\{ a^{(i)}, r^{(i)} \right\}_{i=1}^{t-1},$$

the posterior over the means of the bandit is defined as:

$$\pi\left(\cdot \mid \mathcal{H}^{t-1}\right),$$

where $\pi(\cdot)$ is conditioned on the observed history.

At each timestep t, Thompson sampling samples an estimate $\tilde{\mu}_k^{(t)}$ of the mean μ_k from each posterior k and ranks these samples to select the arm with the highest sampled mean. By sampling from the posterior, Thompson sampling uses the uncertainty of the mean to balance exploration and exploitation. As it is playing an arm multiple times, the posterior's uncertainty decreases and Thompson sampling will gear towards the highest ranking arms. As Thompson sampling is able to use prior knowledge, sampling efficiency can be greatly improved. In the context of epidemic decision making, we can derive such knowledge using epidemiological modelling theory, which we will do for the experimental scenario considered in Section 4.

Boundary Focused Thompson Sampling (BFTS) [33] implements a Thompson sampling variant for m-top exploration. It uses the posterior samples as an estimate for the arm's means, which are ranked as in Thompson sampling.

BFTS strives to recommend the top-m best arms at any given time. To denote the rank of the ρ-ordered arm, we define this operator:

$$\psi_\rho(\tilde{\mu}^{(t)}). \tag{8}$$

BFTS (Algorithm 2) focuses on both sides of the decision boundary for the top-m arms, in order to decrease the uncertainty about arms $a_m^{(t)}$ and $a_{m+1}^{(t)}$ with rankings $\psi_m(\tilde{\mu}^{(t)})$ and $\psi_{m+1}(\tilde{\mu}^{(t)})$, respectively. Therefore, the arms ranked $\psi_m(\tilde{\mu}^{(t)})$ and $\psi_{m+1}(\tilde{\mu}^{(t)})$ are played with equal probability using a Bernoulli experiment. In Appendix B we provide a Bayesian analysis of BFTS. While this analysis does not result in a bound on the simple regret, it does provide additional insight in BFTS' exploration strategy and confirms that this strategy is well-grounded.

Algorithm 2: Boundary Focused Thompson Sampling

Input: $\pi(\cdot)$, $\mathcal{H}^{(0)} = \emptyset$

for $t = 1, \ldots, +\infty$ **do**
- $\tilde{\mu}^{(t)} \sim \pi\left(\cdot \mid \mathcal{H}^{t-1}\right)$
- $b \sim \mathcal{B}er(0.5)$
- $a^{(t)} = \psi_{m+b}(\tilde{\mu}^{(t)})$
- $r^{(t)} \leftarrow$ Pull arm $a^{(t)}$
- $\mathcal{H}^{(t)} \leftarrow \mathcal{H}^{(t-1)} \cup \left\{a^{(t)}, r^{(t)}\right\}$
- Recommend top arms based on $\pi\left(\cdot \mid \mathcal{H}^{t-1}\right)$

end

4 Vaccine policy evaluation

SARS-CoV-2 has emphasised the importance of pandemic control [37]. This virus manifests in distinct clinical outcomes, ranging from asymptomatic infection to COVID-19 disease, which may induce mild to severe symptoms [49, 37]. Severe COVID-19 cases require hospitalisation and might result in a fatal outcome [53, 37]. As of August 2022, over 572 million confirmed cases and 6.3 million deaths were reported. Since the end of 2019, new variants of SARS-CoV-2 have emerged. The first major mutation, D614G, induced an increased transmissibility and infectiousness, making it the dominant strain of the virus globally [61]. Subsequently, a series of Variants of Concern (VoC) emerged which further increased transmissibility and/or disease severity [8]. Alpha VoC, Beta VoC and Gamma VoC were detected near the end of 2020.

To avoid the overflow of hospitals and to reduce mortality, strategies to reduce the number of infections were necessary. In the first phase of the pandemic, such measures were limited to imposing contact reductions [1]. In a later phase of the pandemic, vaccines became available [37].

Early 2020, the first COVID-19 vaccines were developed, where mRNA vaccines and vector-based vaccines were first to show promising results [6, 14, 9]. In this work we focus on learning optimal policies to allocate vaccines to a large population when vaccines become available in limited batches, due to the gradual production of vaccines. As vaccines are administered gradually, certain contact reductions need to be kept in place during the vaccination campaign. Therefore we evaluate vaccine allocation strategies under different contact reduction scenarios in our experiments. We investigate how to organize COVID-19 vaccine allocation policies while minimising infections and hospitalisations. We explore different determinants regarding vaccine allocation policies, including the targeted age group and the vaccine type (i.e., mRNA and vector-based), which results in a large number of preventive policies that is to be evaluated.

In this work, we model the Belgian COVID-19 epidemic using the STRIDE individual-based simulator [30], that explicitly models 11 million Belgians [54]. We consider the phase of the COVID-19 epidemic where vaccine supplies started to be delivered on a weekly basis, with a changing supply rate as vaccine production increased over time. We take into account the two types of vaccines that were available in Belgium during this phase, i.e., mRNA [40, 60] and vector-based vaccines [62]. We investigate how a weekly supply of vaccines is best allocated to all age groups that make up the population. We consider different social distancing schemes to explore the effect of such policies on the vaccination campaign. In these scenarios, we investigate the impact of policies on infections and hospitalisations. To enable a Bayesian learning approach, we will introduce priors for these scenarios using epidemic modelling theory in Section 4.3.

4.1 STRIDE model and configuration

In our experiments, we start the simulation period on January 1st 2021, when the first vaccines become available. We note that at this time, the circulating variant in Belgium was the Alpha VoC. We use the individual-based model STRIDE to simulate the entire Belgian population of 11 million individuals. A single simulation considers 4 calendar months, from January 1st 2021 until May 1st 2021, and includes holidays. The vaccination strategy linked to the pulled arm is applied each day of the simulation, resulting in an aggregate reward at the end of the simulation. Depending on the scenario, a distinct regimen of contact reductions is imposed on the population. Imposing a higher contact reduction means individuals can participate in fewer person-to-person contacts, thereby reducing the likelihood to acquire infection. To compare different vaccination strategies, we keep the contact reductions constant over the entire simulation. Moreover, contact tracing is performed every day. Additional details on the contact tracing configuration can be found in Appendix C.

Because we simulate the progress of the pandemic starting from January 1st 2021 and not from the start of the pandemic, the population is initialised with the proportion of immunity that was estimated at that moment in Belgium. This proportion of immunity was estimated using the stochastic compartment model by Abrams et al. [1]. We consider the Alpha VoC variant of SARS-CoV-2,

which is 50% more infectious compared to previously circulating variants [44].

As the appropriate vaccination strategy will depend on imposed contact reductions, we consider different scenarios as specified in Table 1. Each scenario is characterised by distinct contact reductions for schools (primary c_p, secondary c_s, tertiary c_t), workplace c_w and community c_c.

Scenario	c_p	c_s	c_t	c_w	c_c
Baseline	0%	50%	100%	70%	70%
Relaxed	0%	50%	100%	50%	50%
Tertiary Education	0%	50%	70%	70%	70%
Secondary Schools	0%	0%	100%	70%	70%
Relaxed Community	0%	50%	100%	70%	50%
Relaxed Workplace	0%	50%	100%	50%	70%

Table 1: Epidemic scenarios for COVID-19 with different contact reductions imposed. 0% implies there is no reduction in contacts and 100% means imposing full contact reduction.

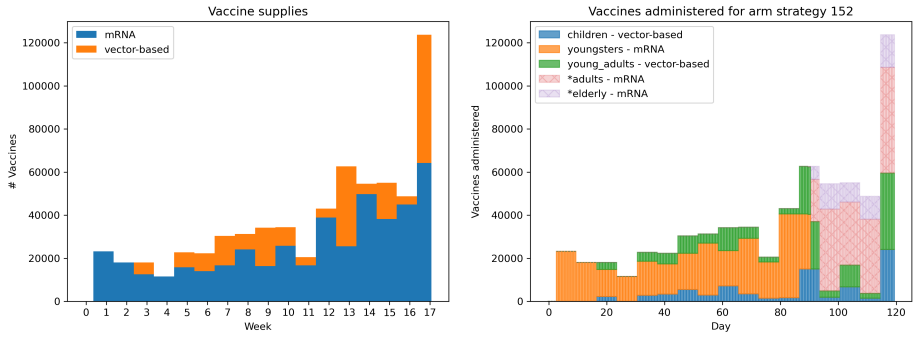
4.2 Vaccine allocation

Our setup incorporates two types of vaccines: mRNA vaccines and vector-based vaccines [38]. The BNT162b2 vaccine by Pfizer-BioNTech and the mRNA-1273 by Moderna are grouped as mRNA vaccines. Analogously, AZD1222 by Oxford-AstraZeneca and Ad26COV2S by Janssen are both grouped as vector-based vaccines.

Each simulation day, a certain number of vaccines is allocated to a selection of individuals. Our simulation is based on the reported supply of mRNA and vector-based vaccines delivered in Belgium since January 1, 2021 [47]. As this concerns a retrospective analysis, the delivery dates and quantities are known. To allow vaccinations every day, the supplied vaccines are divided uniformly over the respective week (Figure 1a).

The vaccination strategy is kept fixed over all simulation days. We define a vaccination strategy as a quintuple of the different vaccine types, divided over 5 age groups: Children (0-4), Youngsters (5-18), Young Adults (19-25), Adults (26-64) and Elderly (65+).

For the vaccine to reach its full protection, it requires some time after its administration, as neutralizing antibodies and virus-specific T cells must be produced [45]. We model this effect using a linear activation function. The vaccine activation function will linearly complete its protection over a given time span, that starts at the time when the first dose of the vaccine is administered. We assume the vaccine's maximum efficacy will be reached after 6 weeks, to mimic the full vaccination scheme, where maximum efficacy is expected 2 weeks



(a) (b)

Figure 1: (a) Stacked bar chart of the vaccine supply from January 1st 2021 [47]. (b) Example strategy: The strategy starts by vaccinating children and young adults with vector-based vaccines and youngsters with mRNA vaccines.

after the second vaccine dose [9].[1] We adopt vaccine efficacies published at the time when the vaccination policies were being devised. For the mRNA vaccines, we assume a vaccine efficacy $VE_S = 95\%$ for the susceptibility, $VE_I = 95\%$ for infectiousness and $VE_D = 100\%$ for the propensity to protect from severe disease [40]. For the vector-based vaccines we assume $VE_S = 67\%$, $VE_I = 67\%$ and $VE_D = 100\%$ [29].

At every simulation day, each of the age groups can be allocated one of the two vaccine types (i.e., mRNA or vector-based) or no vaccine. When vaccinating the population according to a vaccination strategy, STRIDE randomly selects unvaccinated individuals of the appropriate age groups to vaccinate. The number of vaccines per age group is specified based on the real vaccine supply. This supply is proportionally distributed to the different age groups based on their respective sizes. When all members of a particular age group are vaccinated, the vaccines will be divided among the other age groups, prioritizing age groups with the same vaccine type assigned. This ensures that no vaccines are wasted in the simulation. As an example, we present the vaccine administration for one of the evaluated strategies in Figure 1b.

4.3 Disease outbreak outcomes

A disease outbreak has two possible outcomes: either it is able to spread beyond a local context and becomes a fully established epidemic or it fades out [51]. Most stochastic epidemiological models reflect this reality and hence its epidemic size distribution is bimodal [51]. In the context of this study, where we consider an ongoing COVID-19 epidemic, we can focus on the mode of the infection size distribution that is associated with the established epidemic. This distribution

[1] For the Janssen vector-based vaccine, only one dose was administered. As these vector-based vaccines have a similar working mechanism, we assume the same activation function.

is known to be approximately Gaussian [35, 7]. We note that this argument does not automatically hold for the hospitalisation size distribution, which we also consider in our experiments. The reason for this is that, as for many infectious diseases, the likelihood to be hospitalised is not uniformly distributed across the population [36]. For COVID-19, it is known that hospitalisation rates rise exponentially with age [39]. Nonetheless, as for a particular arm, we keep the contact reductions and vaccine policy constant, we still expect a central trend that can be well approximated with a Gaussian.

To incorporate this prior knowledge in BFTS, we consider the reward distribution Gaussian with unknown mean and variance and assume an uninformative Jeffreys prior $(\sigma)^{-3}$ on (μ, σ^2) [24]. This prior leads to the non-standardised t-distributed posterior, that we truncate on the interval $[0, 1]$ as we know the arm's means are in this interval. The formal derivation for this posterior can be found in Appendix A.

4.4 COVID-19 bandit

In the COVID-19 setting, we aim to find the prevention strategy that minimizes the attack rate, with regards to infections or hospitalisations. The attack rate in terms of infections (ARI) is the proportion of the population that was infected at the end of the simulation. The hospitalisation attack rate (ARH) corresponds to the proportion of the population hospitalised at the end of the simulation. To minimize the attack rate, we take the complement as a reward signal: $1 - ARI$ for infections and $1 - ARH$ for hospitalisations.

Given the 5 age groups and 2 vaccine types, with no vaccine as a third option, the bandit would have a total of 3^5 arms. In order not to waste any vaccines, we disregard all arms that do not use both types of vaccines, which results in a bandit with 180 arms.

While the bandit learns, it pulls an arm based on its sampling strategy. This arm is then translated to a corresponding vaccination strategy for each of the age groups. When pulling an arm, the bandit runs a STRIDE simulation for 4 calendar months, where the chosen vaccination strategy is executed each day until the end of the simulation.

4.5 Establishing a ground truth to evaluate the framework

To validate our method, we establish a baseline scenario (Table 1) where we simulate all strategies 100 times to identify the true set of optimal arms, to which we will refer as the *ground truth*. This ground truth will be used to measure the performance of the algorithms with regards to their ability to identify the true set of optimal arms. Figure 2 shows the reward distributions for 100 simulations of all arms.

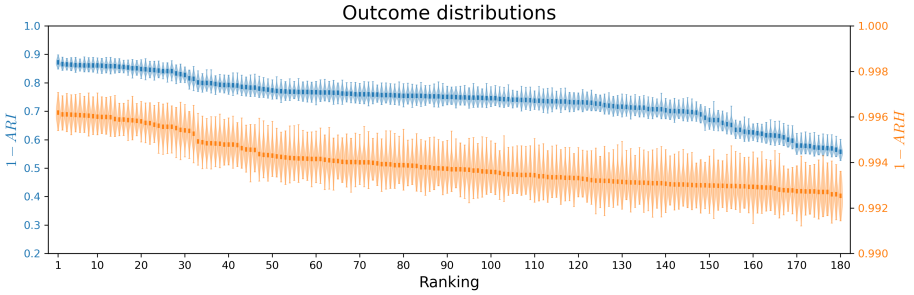


Figure 2: Ground truth of all arms for the baseline scenario, ranked based on infections (1 - ARI) (as shown in blue) and hospitalisations (1 - ARH) (as shown in orange).

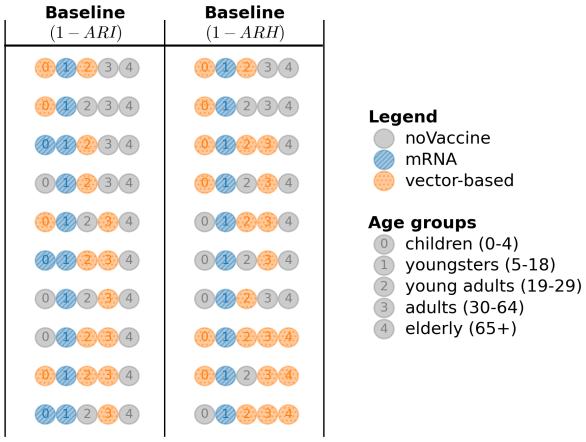


Figure 3: True top-10 vaccination strategies for the baseline scenario for minimising the infection (ARI) and hospitalisation (ARH) attack rates.

The true top-10 vaccination strategies follow a distinct trend for the infection attack rate ARI (Figure 3). Most noticeably, all 10 strategies prioritise vaccinating youngsters with mRNA vaccines. Children do not receive a particular recommendation in the top-10 strategies. Both young adults and adults receive vector-based vaccines if they are prioritised, while elderly are not assigned any vaccine. However, we note that any remaining vaccines will be divided over the remainder of the unvaccinated population. Therefore, elderly will eventually be vaccinated, given these strategies after the target age groups have been finished.

For the scenario that considers the hospital attack rate, we observe a different set of top allocation policies (Figure 3). Note that there is some overlap between the strategies for ARI and ARH, as reducing overall infections helps to reduce hospitalisations. Youngsters are still prioritised for the mRNA vaccines. However, all other age groups are given vector-based vaccines.

Using this ground truth, we compare the performance of BFTS to AT-LUCB and Uniform sampling. Uniform sampling aims to pull each arm an equal number of times by pulling the least-sampled arm at each timestep. Consequently, uniform sampling recommends the empirical m-top arms. Both the BFTS and AT-LUCB algorithm are described in Section 3.2. We report the algorithms' performances using two statistics [25]: the sum of the means of the m-top arms at time t

$$\sum_{a \in J^{(t)}} \mu_a, \tag{9}$$

and the proportion of correctly recommended arms at time t

$$\frac{|J^{(t)} \cap J^{\text{True}}|}{m}. \tag{10}$$

J^{True} denotes the true set of optimal arms, which we know via our ground truth, and $J^{(t)}$ denotes the set of recommended arms at time t.

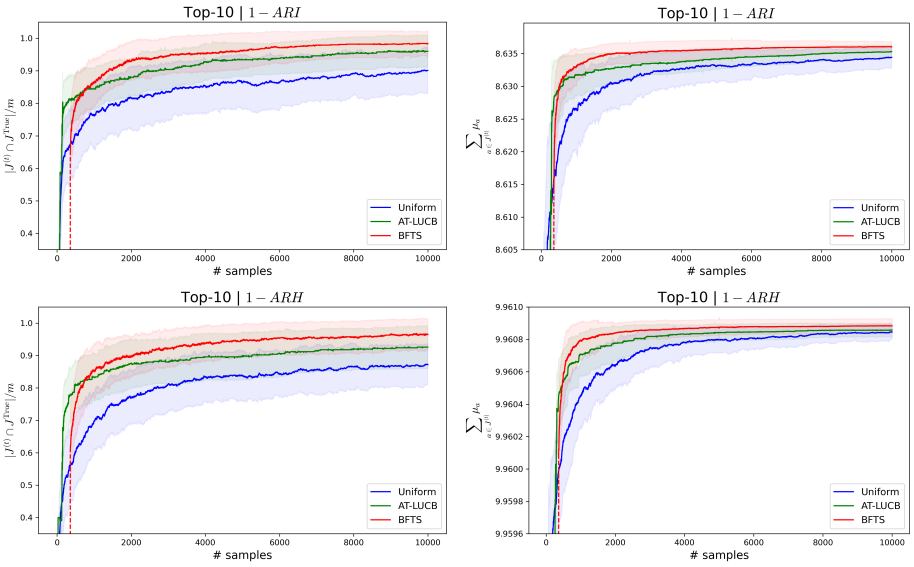
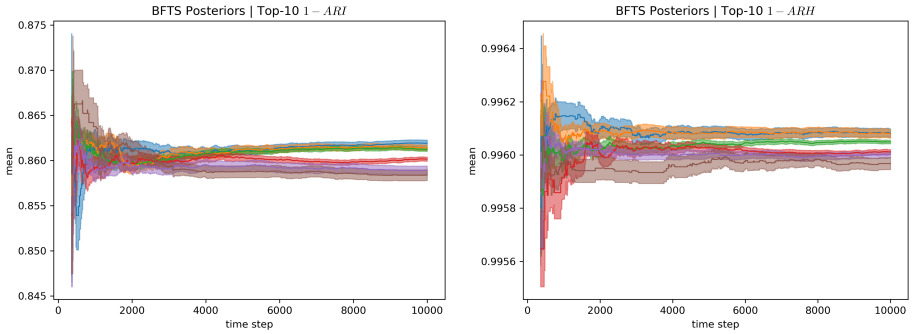


Figure 4: Learning curves for the ground truth based on infections (ARI) and hospitalisations (ARH), top vs bottom row, respectively. Left column: The average proportions of correctly ranked arms, with standard deviation. Right column: The average sum of true means, with standard deviation.

Note that uniform sampling and BFTS obtain one sample per time step, whereas AT-LUCB samples twice per timestep. We plot the results in terms of the number of samples to facilitate a fair comparison. We consider truncated t-distribution posteriors for BFTS (Section 4.3). Figure 4 shows the results for

100 simulations per algorithm for 10.000 samples, in terms of infections and hospitalisations. To obtain a proper posterior, each arm's posterior needs to be initialised two times [24]. In general, BFTS needs this short period to meet AT-LUCB's performance, but quickly outperforms AT-LUCB after this warm-up period.



(a) (b)

Figure 5: Posteriors for the *Baseline* scenario concerning infections (a) and hospitalisations (b). The estimated means and uncertainty (standard deviation) are shown for the 3 arms above and the 3 arms below the decision boundary. Note that the arms closest to the decision boundary have a reduced uncertainty, as the bandit focused on these arms to reduce its uncertainty about the decision boundary.

Figure 5 shows the posteriors' estimated means and uncertainty (standard deviation) for the 3 arms above and the 3 arms below the decision boundary of a single bandit run of BFTS. As the bandit pulls an arm, it reduces its uncertainty for that arm. However, as the means are close to each other (see Figure 2), there still remains uncertainty with regards to the estimated top-10 arms. We note that inspecting the posteriors over time presents an interesting way for decision makers to interpret and report the bandit's recommendations and the uncertainty associated with these recommendations.

4.6 Analysing vaccines policies under various contact reduction schemes

We define a 180-armed bandit to learn the 10 best vaccination strategies using BFTS for the different contact reduction scenarios mentioned above (Table 1). Due to the computational burden of the STRIDE model, running a single simulation takes approximately 5-6 minutes on the Genius VSC[2] high performance computing infrastructure, for our configurations. Each time the bandit pulls an arm, a new simulation is run. Consequently, the time required to perform

[2] `https://www.vscentrum.be`

experiments increases quickly due to the sequential nature of the bandit algorithm. Therefore, we have put a limit of 2000 simulations (i.e., arm pulls) for each experiment, which corresponds to about 1.5 weeks of computation on the Genius VSC high performance computing infrastructure. In the discussion, we consider future work with regards to further scaling the computations.

For the baseline COVID-19 scenario we obtained a ground truth for the bandit to validate our results. Here, we evaluate our bandit framework for what it was intended, to find the top strategies when evaluating each arm is computationally unfeasible. Therefore, as we do not have a ground truth, we evaluate the quality of the obtained results by investigating the bandit's decision uncertainty about the learned top vaccination strategies.

In this analysis, we investigate vaccine allocation strategies under distinct contact reduction policies. The *Relaxed* scenario (Table 1) imposes 50% contact reductions in the workplace and community, with primary schools open at full capacity. Secondary schools operate at 50% capacity, while universities and colleges are closed [54]. This scenario considers moderate restrictions at work and in the community, requiring a well-chosen vaccination strategy to counteract the additional contacts compared to the baseline scenario. In the *Tertiary Education* scenario, we follow the same contact reductions as the baseline, with the exception of having tertiary schools open at 70% contact reductions. The *Secondary Schools* scenario explores the case where primary, secondary schools and universities are open. As the baseline scenario has shown that children should be prioritised when vaccinating, this scenario provides an interesting perspective as school contacts for children and youngsters are fully allowed. The *Relaxed Community* and *Relaxed Workplace* scenarios both consider a middle-ground between the baseline and relaxed scenario. The uncertainty analysis (based on the analysis of the posteriors) for all these scenarios can be found in Appendix D.

When minimising the infection attack rate (ARI), there is a clear trend regarding youngsters and elderly across the scenarios (Figure 6). In all scenarios except the *Relaxed* scenario, the top vaccination strategies exclusively prioritise mRNA vaccines for youngsters. In the *Relaxed* scenario, our analysis recommends to include elderly in the prioritisation and to vaccinate them with vector-based vaccines. As in this scenario, reducing infections is the priority, the best estimated strategies are those that prioritise youngsters, young adults and adults as they are making more contacts compared to the *Baseline* scenario. The *Secondary Schools* and *Relaxed Community* scenarios prioritise elderly people for a few strategies as these are scenarios in which they have more social contacts. For the *Secondary Schools* scenario, as youngsters make more social contacts due to the schools operating at full capacity, they are more likely to be infected and propagate the virus to their families, further increasing the likelihood for the elderly to be infected. There are fewer strategies prioritising elderly compared to youngsters, as youngsters are prioritised in each strategy for the 5 scenarios.

For the hospitalisation attack rate (ARH), we notice a shift in focus for the *Relaxed* and *Relaxed Community* scenarios, where all 10 strategies prioritise giving elderly mRNA vaccines (Figure 7). Both scenarios are more relaxed

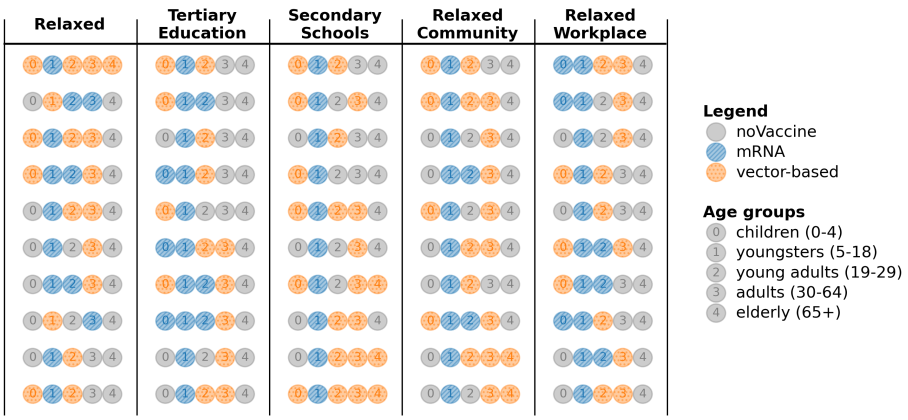


Figure 6: Learned top-10 vaccination strategies when minimising the infection attack rate (ARI) under various contact reduction schemes.

when it comes to community contacts, in which the elderly take most part as they do not go to school or work. As the older population is more likely to be hospitalised, the bandit learns to vaccinate them first. While both vaccine types have the same efficacy towards severe disease and as a consequence hospitalisations, the fact that the mRNA vaccines have a higher efficacy for susceptibility and infectiousness, combined with a higher amount of available vaccines during the course of the simulation, renders them the preferred option to vaccinate and protect elderly from being hospitalised. The other scenarios follow similar trends compared to the scenario that considers infections, and as such prioritise mRNA vaccines for youngsters.

Interestingly, these results indicate for each scenario which age group should be prioritised for vaccination as the bandit has learned the best strategies assign mRNA vaccines to that age group. For both ARI and ARH, we notice another trend: if young adults, adults and elderly are prioritised for any of the vaccines, they are assigned vector-based vaccines, with one notable exception. The *Relaxed* and *Relaxed Community* scenarios for ARH are the only exception to this as the elderly are a higher priority as they contribute most to the hospitalisation load. Moreover, the number of arms in the top-10 that prioritise a particular age group also indicates the importance of the choice to vaccinate that age group. For example, in the *Baseline* scenario for ARH, even though hospitalisations were a priority, only three arms prioritise vaccinating the elderly because the impact of other age groups is more important (Figure 3). Analogously, the presence of multiple vaccine types for a group in the top-10 indicates it is less important to prioritise a particular vaccine type for that age group. For example, the *Baseline* scenario for ARI (Figure 3) indicates less importance with regards to the chosen vaccination strategy when it comes to children as mRNA and vector-based vaccines were recommended options. We close by stating that these results greatly depend on the fact that the used vaccines were quite suc-

cessful in reducing the transmission likelihood. With the emergence of variants, these odds changed, which we discuss in the next section.

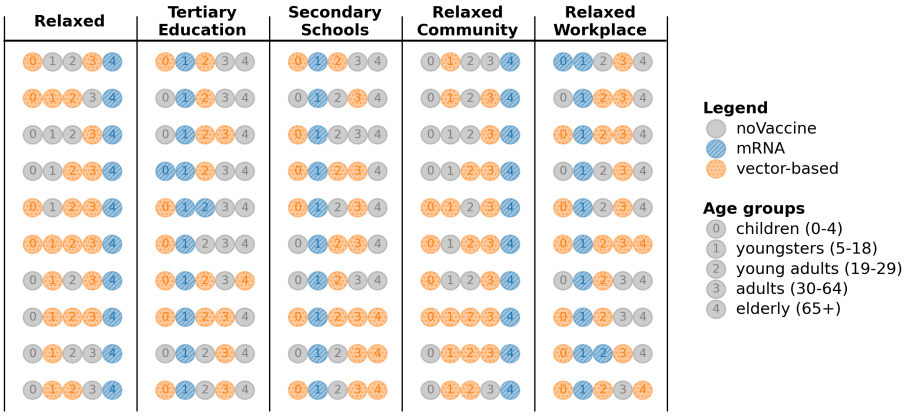


Figure 7: Learned top-10 vaccination strategies when minimising the hospitalisations attack rate (ARH) under various contact reduction schemes.

5 Discussion

In this work, we present a multi-armed bandit framework to study mitigation policies in an individual-based epidemiological model. With this framework, we study vaccine allocation policies in a COVID-19 epidemic. We show it is possible to efficiently learn the best strategies using a limited number of model evaluations. Additionally, the bandit allows policy makers to use the learned posteriors and their uncertainty to make informed decisions. Through our vaccine allocation study, we highlight the impact of contact reductions on vaccine allocation policies.

We assume prevention strategies of equal financial cost, which is a realistic assumption as governments typically operate within budget constraints. For simplicity, we keep contact reductions constant during a simulation. Furthermore, we do not consider imported cases from abroad, motivated by the fact that we consider an ongoing epidemic that is mainly driven by intra-country contact dynamics.

This study concerns a retrospective analysis that assumes that vaccine delivery dates are known. To reason about policies when the delivery scheme of vaccines is uncertain, we consider the use of stateful reinforcement learning for future work.

We note that the vaccine efficacies are representative for the start of the vaccination campaign, but as variants continued to emerge, vaccine efficacy regarding susceptibility and infectiousness has decreased significantly. Nonetheless, our study provides insights to optimal policies at the start of the vaccination

campaign. We consider the evaluation of vaccination policies under the emergence of distinct VoC as future work. Additionally, we consider all age groups in the vaccine allocation study. However, as for the SARS-CoV-2 pandemic new vaccine platforms were trialed, these vaccines were only approved for 18 years and older at the start of vaccination campaign [52]. Our analyses do show that a rapid adoption of vaccines by children and/or youngsters could have an important impact on the epidemic, and could lead to lower contact reductions. This is an important consideration for future vaccination campaigns, which might target children earlier on, as the mRNA and vector-based vaccine platforms have now undergone rigorous evaluation.

We do not account for behavioral changes due to vaccination in this work. In the context of COVID-19, it was shown that individuals increase their contacts once they have been vaccinated [48]. We consider such behavioral aspects an interesting aspect to study in future work. Furthermore, as we consider a limited time period (4 months), we do not consider vaccine waning in this study [15]. We do acknowledge that this would be interesting to consider for future work, when evaluating long term mitigation policies.

In this work, we do not explicitly consider correlations between arms, to establish a generic policy evaluation framework that supports decision uncertainty. We note that the Bayesian exploration scheme will implicitly account for such correlations. While there are bandit algorithms that can exploit such correlations [50, 22, 43], to the best of our knowledge there exist no Bayesian m-top exploration algorithms, which thus constitutes an interesting direction for future work.

Running sequential simulations for the bandit algorithm on STRIDE increases the time needed to conduct experiments. Therefore, our bandits framework would strongly benefit from parallelisation with regards to the pulled arms. We note that an extension of the Bayesian m-top algorithm with a delayed bandit approach constitutes an important venue for subsequent work [18]. Furthermore, additional optimisations for the parallelisation of the STRIDE model on a larger number of CPUs, to reduce the execution time of a single STRIDE simulation even more, could be explored.

In addition to the vaccine allocation policies studied here, our approach can be extended to explore other diseases and mitigation strategies for both disease and transmission, such as antiviral allocation strategies [46]. From an epidemiological perspective, future work may focus on the impact of universal testing approaches to mitigate the epidemic [34]. Similarly, the effect of superspreading [31] and its impact on social distancing and vaccine allocation presents interesting venues for future research.

Acknowledgments

A.C. is funded by the Fonds voor Wetenschappelijk Onderzoek (FWO) via fellowship 1SF7823N and received funding from the Research Council of the Vrije Universiteit Brussel (OZR-VUB) through OZR mandate OZR3819. A.C. also

acknowledges funding from the FWO COVID-19 research project G0H0420N. All experiments were run on the Genius and Hydra clusters of the Flemish Supercomputer Center (Vlaams Supercomputer Centrum - VSC). This work also received funding from the European Research Council (ERC) under the European Union's Horizon 2020 research and innovation program (grant number 101003688 – EpiPose project). P.J.K.L. gratefully acknowledges support from FWO via postdoctoral fellowship 1242021N and the Research council of the Vrije Universiteit Brussel (OZR-VUB via grant number OZR3863BOF). N.H. acknowledges support from the Scientific Chair of Evidence-based Vaccinology under the umbrella of the Methusalem framework at the University of Antwerp. N.H. and A.N. acknowledge funding from the iBOF DESCARTES project (reference: iBOF-21-027). L.W. gratefully acknowledges support from FWO postdoctoral fellowship 1234620N. This research acknowledges funding from the Flemish Government through the AI Research Program. The funders had no role in study design, data collection and analysis, decision to publish, or preparation of the manuscript.

Reproducibility

The code for the bandit framework, the m-top algorithms and the COVID-19 experiments that were conducted in this paper is available at `https://github.com/icimpean/m-top-covid`. The vaccine extension to the STRIDE simulator is available at `https://github.com/icimpean/stride/tree/vaccine`.

References

[1] Steven Abrams, James Wambua, Eva Santermans, Lander Willem, Elise Kuylen, Pietro Coletti, Pieter Libin, Christel Faes, Oana Petrof, Sereina A. Herzog, Philippe Beutels, and Niel Hens. Modelling the early phase of the belgian covid-19 epidemic using a stochastic compartmental model and studying its implied future trajectories. *Epidemics*, 35:100449, 2021.

[2] Jean-Yves Audibert and Sébastien Bubeck. Best arm identification in multi-armed bandits. In *COLT-23th Conference on Learning Theory*, 2010.

[3] Raghav Awasthi, Keerat Kaur Guliani, Saif Ahmad Khan, Aniket Vashishtha, Mehrab Singh Gill, Arshita Bhatt, Aditya Nagori, Aniket Gupta, Ponnurangam Kumaraguru, and Tavpritesh Sethi. Vacsim: Learning effective strategies for covid-19 vaccine distribution using reinforcement learning. *Intelligence-Based Medicine*, 6:100060, 2022.

[4] Nicole E Basta, Dennis L Chao, M Elizabeth Halloran, Laura Matrajt, and Ira M Longini. Strategies for pandemic and seasonal influenza vaccination of schoolchildren in the United States. *American journal of epidemiology*, 170(6):679–686, 2009.

[5] Robert E Bechhofer. A sequential multiple-decision procedure for selecting the best one of several normal populations with a common unknown variance, and its use with various experimental designs. *Biometrics*, 14(3):408–429, 1958.

[6] Emily Bettini and Michela Locci. Sars-cov-2 mrna vaccines: Immunological mechanism and beyond. *Vaccines (Basel)*, 9(2), Feb 2021.

[7] Tom Britton. Stochastic epidemic models: a survey. *Mathematical biosciences*, 225(1):24–35, 2010.

[8] CDC. SARS-CoV-2 Variant Classifications and Definitions. `https://www.cdc.gov/coronavirus/2019-ncov/variants/variant-classifications.html#concern`.

[9] CDC. Stay Up to Date with Your COVID-19 Vaccines. `https://www.cdc.gov/coronavirus/2019-ncov/vaccines/stay-up-to-date.html`.

[10] Dennis L. Chao, Scott B. Halstead, M. Elizabeth Halloran, and Ira M. Longini. Controlling Dengue with Vaccines in Thailand. *PLoS Neglected Tropical Diseases*, 6(10), 2012.

[11] Olivier Chapelle and Lihong Li. An empirical evaluation of thompson sampling. In *Advances in neural information processing systems*, pages 2249–2257, 2011.

[12] S.G. Eubank, V.S.a. Kumar, M.V. Marathe, A. Srinivasan, and N. Wang. Structure of social contact networks and their impact on epidemics. *DIMACS Series in Discrete Mathematics and Theoretical Computer Science*, 70(0208005):181, 2006.

[13] Eyal Even-Dar, Shie Mannor, and Yishay Mansour. Action elimination and stopping conditions for the multi-armed bandit and reinforcement learning problems. *Journal of machine learning research*, 7(Jun):1079–1105, 2006.

[14] FDA. COVID-19 Vaccines. `https://www.fda.gov/emergency-preparedness-and-response/coronavirus-disease-2019-covid-19/covid-19-vaccines`.

[15] Jill M Ferdinands, Suchitra Rao, Brian E Dixon, Patrick K Mitchell, Malini B DeSilva, Stephanie A Irving, Ned Lewis, Karthik Natarajan, Edward Stenehjem, Shaun J Grannis, Jungmi Han, Charlene McEvoy, Toan C Ong, Allison L Naleway, Sarah E Reese, Peter J Embi, Kristin Dascomb, Nicola P Klein, Eric P Griggs, I-Chia Liao, Duck-Hye Yang, William F Fadel, Nancy Grisel, Kristin Goddard, Palak Patel, Kempapura Murthy, Rebecca Birch, Nimish R Valvi, Julie Arndorfer, Ousseny Zerbo, Monica Dickerson, Chandni Raiyani, Jeremiah Williams, Catherine H Bozio, Lenee Blanton, Ruth Link-Gelles, Michelle A Barron, Manjusha Gaglani, Mark G Thompson, and Bruce Fireman. Waning of vaccine effectiveness against moderate and severe covid-19 among adults in the us from the vision network: test negative, case-control study. *BMJ*, 379, 2022.

[16] Neil M Ferguson, Derek A T Cummings, Simon Cauchemez, Christophe Fraser, and Others. Strategies for containing an emerging influenza pandemic in Southeast Asia. *Nature*, 437(7056):209, 2005.

[17] Laura Fumanelli, Marco Ajelli, Stefano Merler, Neil M. Ferguson, and Simon Cauchemez. Model-Based Comprehensive Analysis of School Closure Policies for Mitigating Influenza Epidemics and Pandemics. *PLoS Computational Biology*, 12(1), 2016.

[18] Manegueu Anne Gael, Claire Vernade, Alexandra Carpentier, and Michal Valko. Stochastic bandits with arm-dependent delays. In Hal Daumé III and Aarti Singh, editors, *Proceedings of the 37th International Conference on Machine Learning*, volume 119 of *Proceedings of Machine Learning Research*, pages 3348–3356. PMLR, 13–18 Jul 2020.

[19] Aurélien Garivier and Emilie Kaufmann. Optimal best arm identification with fixed confidence. In *Conference on Learning Theory*, pages 998–1027, 2016.

[20] T. C. Germann, K. Kadau, I. M. Longini, and C. A. Macken. Mitigation strategies for pandemic influenza in the United States. *Proceedings of the National Academy of Sciences*, 103(15):5935–5940, 2006.

[21] Hagit Grushka-Cohen, Raphael Cohen, Bracha Shapira, Jacob Moran-Gilad, and Lior Rokach. A framework for optimizing COVID-19 testing policy using a multi armed bandit approach. *CoRR*, abs/2007.14805, 2020.

[22] Samarth Gupta, Shreyas Chaudhari, Gauri Joshi, and Osman Yağan. Multi-armed bandits with correlated arms. *IEEE Transactions on Information Theory*, 67(10):6711–6732, 2021.

[23] Matthew Hoffman, Bobak Shahriari, and Nando Freitas. On correlation and budget constraints in model-based bandit optimization with application to automatic machine learning. In *Artificial Intelligence and Statistics*, pages 365–374, 2014.

[24] Junya Honda and Akimichi Takemura. Optimality of Thompson Sampling for Gaussian Bandits Depends on Priors. In *AISTATS*, pages 375–383, 2014.

[25] Kwang-Sung Jun and Robert D Nowak. Anytime exploration for multi-armed bandits using confidence information. In *33rd International Conference on Machine Learning*, pages 974–982, 2016.

[26] Shivaram Kalyanakrishnan, Ambuj Tewari, Peter Auer, and Peter Stone. PAC subset selection in stochastic multi-armed bandits. In *ICML*, volume 12, pages 655–662, 2012.

[27] Emilie Kaufmann, Olivier Cappé, and Aurélien Garivier. On the complexity of best arm identification in multi-armed bandit models. *Journal of Machine Learning Research*, 17(1):1–42, 2016.

[28] Emilie Kaufmann and Shivaram Kalyanakrishnan. Information complexity in bandit subset selection. In *Conference on Learning Theory*, pages 228–251, 2013.

[29] Maria Deloria Knoll and Chizoba Wonodi. Oxford-astrazeneca covid-19 vaccine efficacy. *The Lancet*, 397(10269):72–74, 2021.

[30] Elise Kuylen, Sean Stijven, Jan Broeckhove, and Lander Willem. Social contact patterns in an individual-based simulator for the transmission of infectious diseases (stride). *Procedia Computer Science*, 108:2438–2442, 2017. International Conference on Computational Science, ICCS 2017, 12-14 June 2017, Zurich, Switzerland.

[31] Elise J. Kuylen, Andrea Torneri, Lander Willem, Pieter J. K. Libin, Steven Abrams, Pietro Coletti, Nicolas Franco, Frederik Verelst, Philippe Beutels, Jori Liesenborgs, and Niel Hens. Different forms of superspreading lead to different outcomes: heterogeneity in infectiousness and contact behavior relevant for the case of sars-cov-2. *PLOS Computational Biology*, 2022 (In press).

[32] Pieter Libin, Arno Moonens, Timothy Verstraeten, Fabian Ramiro Perez Sanjines, Niel Hens, Philippe Lemey, and Ann Nowe. Deep reinforcement learning for large-scale epidemic control. In Yuxiao Dong, Georgiana Ifrim, Dunja Mladenić, Craig Saunders, and Sofie Van Hoecke, editors, *Machine Learning and Knowledge Discovery in Databases. Applied Data Science and Demo Track*, volume 5 of *Lecture Notes in Computer Science*, pages 155–170. Springer, 1 2021.

[33] Pieter Libin, Timothy Verstraeten, Diederik M. Roijers, Wenjia Wang, Kristof Theys, and Ann Nowe. Bayesian anytime m-top exploration. In *International Conference on Tools with Artificial Intelligence*, pages 1422–1428, 2019.

[34] Pieter J. K. Libin, Lander Willem, Timothy Verstraeten, Andrea Torneri, Joris Vanderlocht, and Niel Hens. Assessing the feasibility and effectiveness of household-pooled universal testing to control covid-19 epidemics. *PLOS Computational Biology*, 17(3):1–22, 03 2021.

[35] Pieter JK Libin, Timothy Verstraeten, Diederik M Roijers, Jelena Grujic, Kristof Theys, Philippe Lemey, and Ann Nowé. Bayesian best-arm identification for selecting influenza mitigation strategies. In *Joint European Conference on Machine Learning and Knowledge Discovery in Databases*, pages 456–471. Springer, 2018.

[36] Jeffrey Luk, Peter Gross, and William W. Thompson. Observations on Mortality during the 1918 Influenza Pandemic. *Clinical Infectious Diseases*, 33(8):1375–1378, October 2001.

[37] Mafalda N. S. Miranda, Marta Pingarilho, Victor Pimentel, Andrea Torneri, Sofia G. Seabra, Pieter J. K. Libin, and Ana B. Abecasis. A tale of three recent pandemics: Influenza, hiv and sars-cov-2. *Frontiers in Microbiology*, 13, 2022.

[38] Abdou Nagy and Bader Alhatlani. An overview of current covid-19 vaccine platforms. *Computational and Structural Biotechnology Journal*, 19:2508–2517, 2021.

[39] Sam Palmer, Nik Cunniffe, and Ruairí Donnelly. Covid-19 hospitalization rates rise exponentially with age, inversely proportional to thymic t-cell production. *Journal of the Royal Society Interface*, 18(176):20200982, 2021.

[40] Fernando P. Polack, Stephen J. Thomas, Nicholas Kitchin, Judith Absalon, Alejandra Gurtman, Stephen Lockhart, John L. Perez, Gonzalo Pérez Marc, Edson D. Moreira, Cristiano Zerbini, Ruth Bailey, Kena A. Swanson, Satrajit Roychoudhury, Kenneth Koury, Ping Li, Warren V. Kalina, David Cooper, Robert W. Frenck, Laura L. Hammitt, Özlem Türeci, Haylene Nell, Axel Schaefer, Serhat Ünal, Dina B. Tresnan, Susan Mather, Philip R. Dormitzer, Uğur Şahin, Kathrin U. Jansen, and

William C. Gruber. Safety and efficacy of the bnt162b2 mrna covid-19 vaccine. *New England Journal of Medicine*, 383(27):2603–2615, 2020. PMID: 33301246.

[41] Mathieu Reymond, Conor F. Hayes, Lander Willem, Roxana Rădulescu, Steven Abrams, Diederik M. Roijers, Enda Howley, Patrick Mannion, Niel Hens, Ann Nowé, and Pieter Libin. Exploring the pareto front of multi-objective covid-19 mitigation policies using reinforcement learning, 2022.

[42] Daniel Russo. Simple bayesian algorithms for best arm identification. In *Conference on Learning Theory*, pages 1417–1418, 2016.

[43] Rahul Singh, Fang Liu, Yin Sun, and Ness Shroff. Multi-armed bandits with dependent arms, 2020.

[44] Kaiming Tao, Philip L. Tzou, Janin Nouhin, Ravindra K. Gupta, Tulio de Oliveira, Sergei L. Kosakovsky Pond, Daniela Fera, and Robert W. Shafer. The biological and clinical significance of emerging SARS-CoV-2 variants. *Nature Reviews Genetics*, 22(12):757–773, December 2021.

[45] John R Teijaro and Donna L Farber. COVID-19 vaccines: modes of immune activation and future challenges. *Nature Reviews Immunology*, 21(4):195–197, 2021.

[46] Andrea Torneri, Pieter Libin, Joris Vanderlocht, Anne-Mieke Vandamme, Johan Neyts, and Niel Hens. A prospect on the use of antiviral drugs to control local outbreaks of COVID-19. *BMC Medicine*, 18(1):191, June 2020.

[47] Joris Vaesen. Dashboard Covid Vaccinations Belgium. `https://covid-vaccinatie.be/en`.

[48] James Wambua, Neilshan Loedy, Christopher I Jarvis, Kerry LM Wong, Christel Faes, Rok Grah, Bastian Prasse, Frank Sandmann, Rene Niehus, Helen Johnson, W.John Edmunds, Philippe Beutels, Niel Hens, and Pietro Coletti. The influence of covid-19 risk perception and vaccination status on the number of social contacts across europe: insights from the comix study. *medRxiv*, 2022.

[49] Mei-Yue Wang, Rong Zhao, Li-Juan Gao, Xue-Fei Gao, De-Ping Wang, and Ji-Min Cao. Sars-cov-2: Structure, biology, and structure-based therapeutics development. *Frontiers in Cellular and Infection Microbiology*, 10, 2020.

[50] Zhiyang Wang, Ruida Zhou, and Cong Shen. Regional multi-armed bandits. In Amos Storkey and Fernando Perez-Cruz, editors, *Proceedings of the Twenty-First International Conference on Artificial Intelligence and Statistics*, volume 84 of *Proceedings of Machine Learning Research*, pages 510–518. PMLR, 09–11 Apr 2018.

[51] Duncan J Watts, Roby Muhamad, Daniel C Medina, and Peter S Dodds. Multiscale, resurgent epidemics in a hierarchical metapopulation model. *Proceedings of the National Academy of Sciences of the United States of America*, 102(32):11157–11162, 2005.

[52] WHO. Interim statement on COVID-19 vaccination for children and adolescents. `https://www.who.int/news/item/24-11-2021-interim-statement-on-covid-19-vaccination-for-children-and-adolescents`.

[53] WHO. WHO Coronavirus (COVID-19) Dashboard. `https://covid19.who.int/`.

[54] Lander Willem, Steven Abrams, Pieter J.K. Libin, Pietro Coletti, Elise Kuylen, Oana Petrof, Signe Møgelmose, James Wambua, Sereina A. Herzog, Christel Faes, Philippe Beutels, and Niel Hens. The impact of contact tracing and household bubbles on deconfinement strategies for COVID-19. *Nature Communications*, 12(1):1–9, 2021.

[55] Lander Willem, Sean Stijven, Ekaterina Vladislavleva, Jan Broeckhove, Philippe Beutels, and Niel Hens. Active Learning to Understand Infectious Disease Models and Improve Policy Making. *PLoS Comput Biol*, 10(4):e1003563, 2014.

[56] Joseph T Wu, Steven Riley, Christophe Fraser, and Gabriel M Leung. Reducing the impact of the next influenza pandemic using household-based public health interventions. *PLoS medicine*, 3(9):e361, 2006.

[57] Reza Yaesoubi and Ted Cohen. Dynamic health policies for controlling the spread of emerging infections: Influenza as an example. *PLOS ONE*, 6(9):1–11, 09 2011.

[58] Reza Yaesoubi and Ted Cohen. Identifying dynamic tuberculosis case-finding policies for hiv/tb coepidemics. *Proceedings of the National Academy of Sciences*, 110(23):9457–9462, 2013.

[59] Reza Yaesoubi and Ted Cohen. Identifying cost-effective dynamic policies to control epidemics. *Statistics in medicine*, 35(28):5189—5209, December 2016.

[60] Na-Na Zhang, Xiao-Feng Li, Yong-Qiang Deng, Hui Zhao, Yi-Jiao Huang, Guan Yang, Wei-Jin Huang, Peng Gao, Chao Zhou, Rong-Rong Zhang, Yan Guo, Shi-Hui Sun, Hang Fan, Shu-Long Zu, Qi Chen, Qi He, Tian-Shu Cao, Xing-Yao Huang, Hong-Ying Qiu, Jian-Hui Nie, Yuhang Jiang, Hua-Yuan Yan, Qing Ye, Xia Zhong, Xia-Lin Xue, Zhen-Yu Zha, Dongsheng Zhou, Xiao Yang, You-Chun Wang, Bo Ying, and Cheng-Feng Qin. A thermostable mrna vaccine against covid-19. *Cell*, 182(5):1271–1283.e16, 2020.

[61] Bin Zhou, Tran Thi Nhu Thao, Donata Hoffmann, Adriano Taddeo, Nadine Ebert, Fabien Labroussaa, Anne Pohlmann, Jacqueline King, Silvio Steiner, Jenna N. Kelly, Jasmine Portmann, Nico Joel Halwe, Lorenz Ulrich, Bettina Salome Trüeb, Xiaoyu Fan, Bernd Hoffmann, Li Wang, Lisa Thomann, Xudong Lin, Hanspeter Stalder, Berta Pozzi, Simone de Brot, Nannan Jiang, Dan Cui, Jaber Hossain, Malania M. Wilson, Matthew W. Keller, Thomas J. Stark, John R. Barnes, Ronald Dijkman, Joerg Jores, Charaf Benarafa, David E. Wentworth, Volker Thiel, and Martin Beer. Sars-cov-2 spike d614g change enhances replication and transmission. *Nature*, 592(7852):122–127, 2021.

[62] Feng-Cai Zhu, Yu-Hua Li, Xu-Hua Guan, Li-Hua Hou, Wen-Juan Wang, Jing-Xin Li, Shi-Po Wu, Bu-Sen Wang, Zhao Wang, Lei Wang, Si-Yue Jia, Hu-Dachuan Jiang, Ling Wang, Tao Jiang, Yi Hu, Jin-Bo Gou, Sha-Bei Xu, Jun-Jie Xu, Xue-Wen Wang, Wei Wang, and Wei Chen. Safety, tolerability, and immunogenicity of a recombinant adenovirus type-5 vectored covid-19 vaccine: a dose-escalation, open-label, non-randomised, first-in-human trial. *The Lancet*, 395(10240):1845–1854, 2020.

arXiv:2301.12822v1 [cs.LG] 30 Jan 2023

Appendices

A Truncated t-distribution

We consider a Gaussian reward distribution with unknown variance and assume an uninformative Jeffreys prior $(\sigma)^{-3}$ on (μ, σ^2). Given rewards $\mathbf{r} = \{r_1, ..., r_n\}$, this prior leads to the non-standardised t-distributed posterior, that we truncate given that we know that the arms' means are in $[0, 1]$:

$$\mu \sim \mathcal{T}_{n,[0,1]}\left(\mu_0 = \frac{\sum_{i=1}^n r_i}{n}, \sigma_0^2 = \frac{\sum_{i=1}^n (r_i - \mu_0)^2}{n^2}\right). \tag{1}$$

Given the pdf $f(\cdot)$ of a non-standardised t-distribution $\mathcal{T}_\upsilon(\mu, \sigma^2)$

$$f(x) = \frac{\Gamma\left(\frac{\upsilon+1}{2}\right)}{\sigma\sqrt{\upsilon\pi}\Gamma\left(\frac{\upsilon}{2}\right)}\left(1 + \frac{(x-\mu)^2}{\upsilon\sigma^2}\right)^{-\frac{\upsilon+1}{2}}, \tag{2}$$

and cdf $F(\cdot)$, we can compute the mean of the truncated non-standardised t-distribution using this normalised definite integral:

$$\frac{\int_0^1 xf(x)dx}{F(\frac{1-\mu}{\sigma}) - F(\frac{0-\mu}{\sigma})} \tag{3}$$

From this, we can derive an analytic expression by first considering the nominator:

$$\begin{aligned}
&\int_0^1 xf(x)dx \\
&= \int_0^1 x\frac{\Gamma\left(\frac{\upsilon+1}{2}\right)}{\sigma\sqrt{\upsilon\pi}\Gamma\left(\frac{\upsilon}{2}\right)}\left(1 + \frac{(x-\mu)^2}{\upsilon\sigma^2}\right)^{-\frac{\upsilon+1}{2}} dx \\
&= \int_{x=0}^{x=1} \sigma\frac{x-\mu+\mu}{\sigma}\frac{\Gamma\left(\frac{\upsilon+1}{2}\right)}{\sqrt{\upsilon\pi}\Gamma\left(\frac{\upsilon}{2}\right)}\left(1 + \frac{(x-\mu)^2}{\upsilon\sigma^2}\right)^{-\frac{\upsilon+1}{2}} \frac{1}{\sigma}dx, \quad u = \frac{x-\mu}{\sigma}, du = \frac{1}{\sigma}dx \\
&= \int_{u=\frac{0-\mu}{\sigma}}^{u=\frac{1-\mu}{\sigma}} (\sigma u + \mu)\frac{\Gamma\left(\frac{\upsilon+1}{2}\right)}{\sqrt{\upsilon\pi}\Gamma\left(\frac{\upsilon}{2}\right)}\left(1 + \frac{u^2}{\upsilon}\right)^{-\frac{\upsilon+1}{2}} du \\
&= \int_{u=\frac{0-\mu}{\sigma}}^{u=\frac{1-\mu}{\sigma}} \sigma uf(u)du + \int_{u=\frac{0-\mu}{\sigma}}^{u=\frac{1-\mu}{\sigma}} \mu f(u)du
\end{aligned} \tag{4}$$

Substituting this in Equation 3, we have:

$$\begin{aligned}
&\frac{\int_{u=\frac{0-\mu}{\sigma}}^{u=\frac{1-\mu}{\sigma}} \sigma uf(u)du + \int_{u=\frac{0-\mu}{\sigma}}^{u=\frac{1-\mu}{\sigma}} \mu f(u)du}{F(\frac{1-\mu}{\sigma}) - F(\frac{0-\mu}{\sigma})} \\
&= \sigma\mathbb{E}\left[u \mid \frac{-\mu}{\sigma} \leq u \leq \frac{1-\mu}{\sigma}\right] + \mu
\end{aligned} \tag{5}$$

B Bayesian analysis of BFTS

This section performs a Bayesian analysis of BFTS [2], motivating its *pure exploration* strategy. We present two heuristics that form the basis of BFTS's exploration strategy, related to their probability of error.

In this Bayesian framework, we reason about the full distribution over bandits. Consequently, the actual means $\boldsymbol{\mu}$ are unknown, and we assert our belief over $\boldsymbol{\mu}$ given

$$\pi(\cdot \mid \mathcal{H}^{(t-1)}), \tag{6}$$

i.e., the prior belief over the means $\pi(.)$ conditioned on the observed history

$$\mathcal{H}^{(t-1)} = \left\{a^{(i)}, r^{(i)}\right\}_{i=1}^{t-1} \tag{7}$$

at time t.

We define $\Psi_\rho(\boldsymbol{\theta}^{(t)})$ to be the ρ ordered arm. We specify the random variables A_ρ^π as the ρ-ranked arms according to the prior belief, and A_ρ^{TS} as the ρ-ranked arm according to Thompson sampling (TS):

$$\begin{aligned} A_\rho^\pi &= \Psi_\rho(\boldsymbol{\mu}) \\ A_\rho^{TS} &= \Psi_\rho(\boldsymbol{\theta}^{(t)}) \end{aligned} \tag{8}$$

As TS is a *probability matching* algorithm [1, 3], it samples directly from the belief asserted in Equation 6. Formally, this is defined as:

$$P(A_\rho^{TS} = \cdot \mid \mathcal{H}^{(t-1)}) = P(A_\rho^\pi = \cdot \mid \mathcal{H}^{(t-1)}) \tag{9}$$

We define $\rho^+ \in [1, \ldots, m]$ and $\rho^- \in [m+1, \ldots, K]$. Using this notation, we can express the true optimal arm set J^* and recommended arm set J^{TS} as:

$$\begin{aligned} J^* &= \{A_{\rho^+}^\pi \mid \forall \rho^+\} \\ J^{TS} &= \{A_{\rho^+}^{TS} \mid \forall \rho^+\}, \end{aligned} \tag{10}$$

we refer to $\overline{J^*}$ as the complement of J^*, i.e., the set of all arms excluding J^*. Note that, both J^* and J^{TS} are random variables, as they are expressed as a union of random variables. We use $P_t(.)$ to denote a probability that is conditioned on the observed history $\mathcal{H}^{(t-1)}$ at time t:

$$P_t(.) = P(. \mid \mathcal{H}^{(t-1)}) \tag{11}$$

Given this framework, we identify two heuristics that underlie BFTS' sampling strategy.

Heuristic 1 *The expectation that BFTS wrongly ranks an arm that is believed to be optimal is bounded by the probability that BFTS wrongly ranks the arm on the sub-optimal side of the decision boundary:*

$$\mathop{\mathbb{E}}_{\rho^-}[P_t(A_{\rho^-}^{TS} \in J^*)] \leq P_t(A_{m+1}^{TS} \in J^*) \tag{12}$$

Given this inequality, we expect that sampling the $m+1$-th arm will reduce $\mathbb{E}_{\rho^-}[P_t(A_{\rho^-}^{TS} \in J^*)]$.

Heuristic 2 *The expectation that BFTS wrongly ranks an arm that is believed to be sub-optimal is bounded by the probability that BFTS wrongly ranks the arm ranked on the optimal side of the decision boundary.*

$$\mathop{\mathbb{E}}_{\rho^+}[P_t(A^{TS}_{\rho^+} \in \overline{J^*})] \leq P_t(A^{TS}_m \in \overline{J^*}) \tag{13}$$

Given this inequality, we expect that sampling the m-th arm will reduce $\mathbb{E}_{\rho^+}[P_t(A^{TS}_{\rho^+} \in \overline{J^*})]$.

These heuristics stem from the fact that it is counter-intuitive for TS to often order an arm as optimal when it is *believed* to be sub-optimal. However, due to the stochastic nature of both the bandit and TS, it is possible to end up with a posterior for which the heuristics do not hold. Notwithstanding, we argue that given the intuition behind probability matching, such events become unlikely when reasonable priors are chosen and BFTS' exploration strategy is followed.

We now show how the expectations in the heuristics relate to the probability of error. As such, given the heuristics, we can bound the probability of error with respect to both sides of the decision boundary (i.e., A^{TS}_{m+1} and A^{TS}_m), demonstrating that BFTS' exploration strategy is well-grounded.

First, we derive the bound in terms of A^{TS}_{m+1}:

$$\begin{aligned}
P_t\left(J^* \neq J^{TS}\right) &= P_t\left(\bigvee_{\rho^-} A^{TS}_{\rho^-} \in J^*\right) \\
&\leq \sum_{\rho^-} P_t\left(A^{TS}_{\rho^-} \in J^*\right) \\
&= \frac{\sum_{\rho^-} P_t\left(A^{TS}_{\rho^-} \in J^*\right) \cdot (K-m)}{(K-m)} \\
&= \mathop{\mathbb{E}}_{\rho^-}\left[P_t\left(A^{TS}_{\rho^-} \in J^*\right)\right] \cdot (K-m) \\
&\overset{(H1)}{\leq} P_t\left(A^{TS}_{m+1} \in J^*\right) \cdot (K-m)
\end{aligned} \tag{14}$$

In the first step, we express the probability of error in terms of the arms that are ranked as sub-optimal by TS. In the second step, we apply a union bound. In the third and fourth step, we transform the sum to an expected value. In the final step, we apply Heuristic 1 ($H1$).

Following analogous arguments, we derive the bound in terms of A^{TS}_m by applying Heuristic 2 (full derivation in Supplementary Information):

$$P_t\left(J^* \neq J^{TS}\right) \leq P_t\left(A^{TS}_m \in \overline{J^*}\right) \cdot m \tag{15}$$

These insights motivate a uniform selection of the two arms on both sides of the decision boundary, as is reflected in BFTS (see Algorithm 2, line 2 and 3 in the for loop).

The BFTS algorithm is constructed such that its sampling strategy is completely independent of its recommendation strategy. Likewise, in this analysis, we consider the belief that BFTS maintains over the problem, in terms of the random variable J^{TS} (Equation 10), rather than the statistic that is used to make recommendations (e.g., the mean of the posterior in our experiments). This observation shows that our analysis is independent from the statistic used to make recommendations with BFTS.

When inspecting other algorithms for the m-top setting, we observe that the decision boundary between the m^{th} and $m+1^{\text{th}}$ arms also plays an important role. For example, the frequentist algorithm AT-LUCB samples two arms each step; the one with the smallest lower-bound among the top-m arms, and the one with the greatest upper-bound among the rest. This is analogous to choosing the optimal and sub-optimal arms that are closest to the decision boundary.

C STRIDE contact tracing configuration

Based on configurations by Willem et al. [4], for contact tracing we assume a 0.7 detection probability with a daily case finding capacity of 10.000 individuals. Tests have a 0.1 probability to be false negative results. There is a 1 day delay for detecting symptomatic individuals and 2 days delay for isolating infected individuals.

D COVID-19 experiments

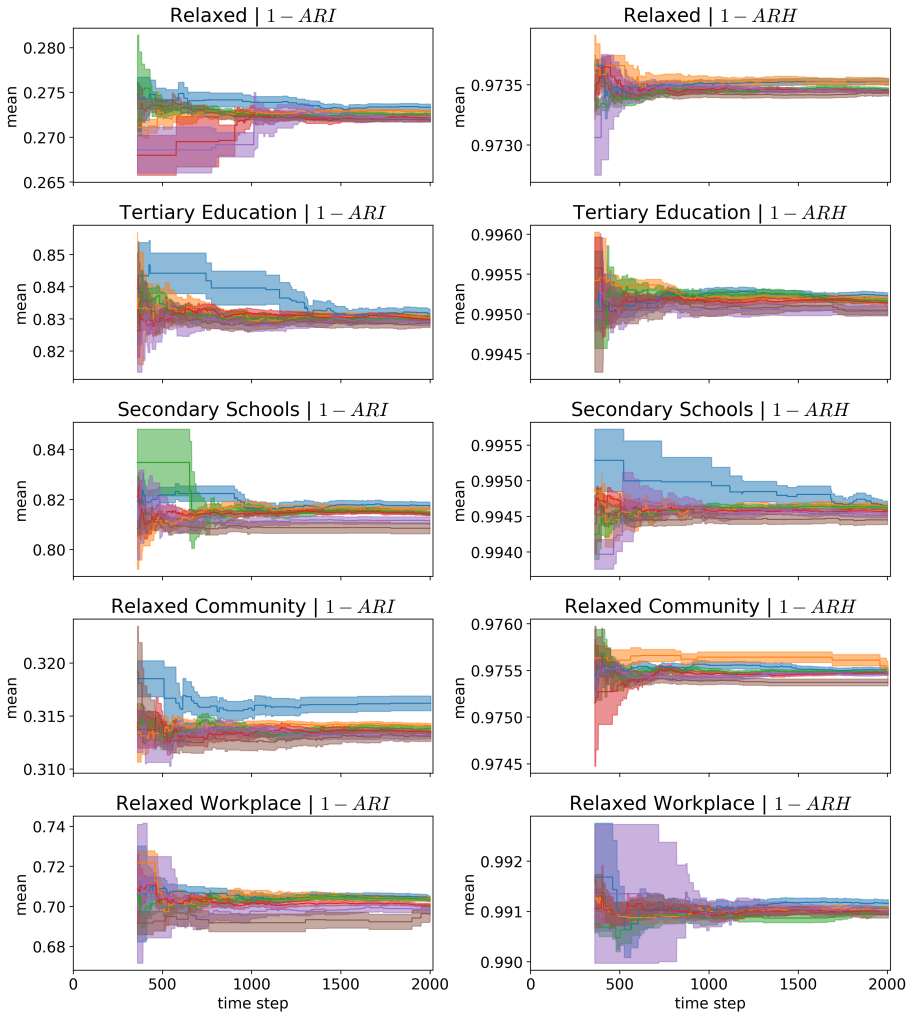


Figure 1: Estimated means and uncertainty (standard deviation) for the 6 arms around the decision boundary. (left) infections ARI. (right) hospitalisations ARH. For the top-10, these are the 8th-13th ranked arms under different contact reduction schemes (Table 1).

References

[1] Shipra Agrawal and Navin Goyal. Analysis of thompson sampling for the multi-armed bandit problem. In *Conference on Learning Theory*, pages 39–1, 2012.

[2] Pieter Libin, Timothy Verstraeten, Diederik M. Roijers, Wenjia Wang, Kristof Theys, and Ann Nowe. Bayesian anytime m-top exploration. In *International Conference on Tools with Artificial Intelligence*, pages 1422–1428, 2019.

[3] Daniel Russo and Benjamin Van Roy. An information-theoretic analysis of thompson sampling. *The Journal of Machine Learning Research*, 17(1):2442–2471, 2016.

[4] Lander Willem, Steven Abrams, Pieter J.K. Libin, Pietro Coletti, Elise Kuylen, Oana Petrof, Signe Møgelmose, James Wambua, Sereina A. Herzog, Christel Faes, Philippe Beutels, and Niel Hens. The impact of contact tracing and household bubbles on deconfinement strategies for COVID-19. *Nature Communications*, 12(1):1–9, 2021.